

AI-assisted experimental measures of entanglement and Bell's nonlocality without state tomography

Patrycja Tulewicz^{1,2,*}, Karol Bartkiewicz^{1,3,*}, Adam Miranowicz^{1,3}, and Franco Nori^{3,4,5}

¹Institute of Spintronics and Quantum Information, Adam Mickiewicz University, PL-61-614 Poznań, Poland

²QSLab: Quantum Software Laboratory, Department of Engineering and Architecture (DIA), University of Parma, Parma, 43124, Italy

³Theoretical Quantum Physics Laboratory, Cluster for Pioneering Research, RIKEN, Wakoshi, Saitama 351-0198, Japan

⁴Center for Quantum Computing, RIKEN, Wakoshi, Saitama 351-0198, Japan

⁵Department of Physics, University of Michigan, Ann Arbor, Michigan 48109-1040, USA

*corresponding authors: Patrycja Tulewicz (pattul@amu.edu.pl), Karol Bartkiewicz (bark@amu.edu.pl)

ABSTRACT

Measuring complex properties in quantum systems, such as various measures of entanglement and Bell nonlocality, is challenging. Traditional methods require a full reconstruction of the density matrix of a given system. An alternative strategy reduces information by using multiple system copies and joint measurements. However, this approach has been considered so far impractical due to difficulties in preparing and controlling multiple quantum-correlated systems and the amplification of experimental noise. Despite these challenges, we have successfully measured two-qubit quantum correlations of Horodecki's and Werner's states using a multicopy approach. We report on experiments with transmon qubits using IBMQ quantum processors to quantify the violation of Bell's inequality and the negativity of a two-qubit entangled state. We compared these results with those from the standard tomography-based approach and developed a maximum likelihood method to reduce the noise. We trained artificial neural networks (ANNs) to estimate entanglement and nonlocality measures from the top five experimental configurations for Werner's and Horodecki's states. The ANN output, based on a reduced set of projections, aligns with expected values and enhances noise robustness. This could simplify and improve the error-robustness of multicopy measurements without complex nonlinear equation analysis. This approach represents a significant advancement in AI-assisted measurements of quantum systems.

Introduction

Quantum entanglement¹⁻³ and Bell's nonlocality, here referred to as the degree of Clauser-Horne-Shimony-Holt (CHSH) inequality violation⁴⁻⁶, are the bedrocks of quantum engineering, quantum information processing⁷, quantum communications (e.g., quantum teleportation)⁸, and quantum cryptography (e.g., quantum key distribution)⁹. Quantum nonlocality has become the foundation for numerous information processing protocols implemented within quantum systems¹⁰⁻¹². Measuring entanglement and Bell's nonlocality helps to validate various predictions of quantum mechanics and ensures that quantum systems behave as expected. At the same time, this pursuit is pushing the boundaries of our experimental capabilities, driving advancements in quantum technologies.

Several detection methods for entanglement and nonlocality have been proposed, such as adaptive approach¹³, collective witness methods utilizing two-copies of a quantum system such as: (i) collectibility¹⁴⁻¹⁸, (ii) a fully-entangled fraction, and (iv) the entropic entanglement witnesses¹⁶. Deep learning techniques¹⁹⁻²¹ have been demonstrated to improve detection and estimation techniques and to enable a precise quantification of entanglement or the degree of the CHSH inequality violation. However, many challenges persist despite advancements made since the groundbreaking experiments conducted by Clauser *et al.*^{22,23} and Aspect *et al.*²⁴⁻²⁶.

Here, we focus on measuring the negativity and Bell's nonlocality for the two-qubit states. We measure the negativity, which is an entanglement measure related to the Peres-Horodecki non-separability criterion^{27,28} and Bell's nonlocality, which corresponds to the optimal violation of the Bell's CHSH inequality²². One of the most commonly used methods determine these quantities is quantum state tomography (QST), which provides complete information about the state under investigation. However, this method has limitations and drawbacks that motivate investigating alternative approaches. QST typically requires numerous measurements (scaling exponentially with the dimension of the measured state), especially for systems with many qubits or continuously varying states, which can be impractical and prohibitively time-consuming. It is highly desirable to consider alternative methods that are experimentally simpler and less resource-intensive than QST, and can be tailored to test

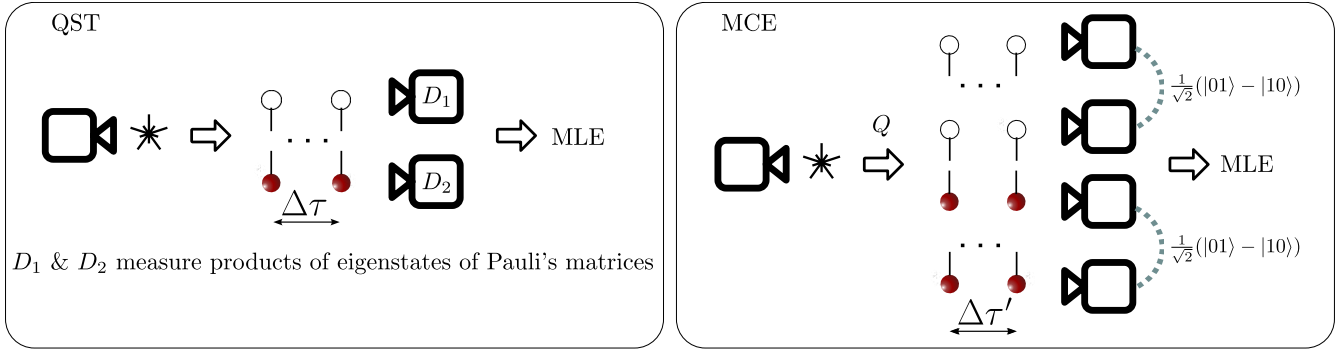


Figure 1. Schematic representation of the approaches based on quantum state tomography (QST) and multicopy estimation (MCE). The symbols $\Delta\tau$ and $\Delta\tau'$ denote the delay time between the generation of each entangled pair or a set of copies of entangled pairs, respectively. The multicopy state generation uses a quantum memory Q to store and release the collected pairs. The detection rates are then processed using maximum likelihood estimation (MLE) to obtain the most probable physical combination of the measured experimental settings.



Figure 2. Examples of graphs representing joint multicopy measurement: (a) the paired single-subsystem singlet projections l_1 , (b) the paired cross-subsystem singlet projections \bar{l}_2 , (c) the chained single-subsystem singlet projections c_3 , and (d) the chained cross-subsystem singlet projections \bar{c}_2 . Black lines combine subsystems (red and white spheres) of the same copy of $\hat{\rho}$, while dotted lines correspond to projections of the multicopy system onto the singlet state.

specific aspects of entanglement and nonlocality relevant to a particular experiment or application. Developing such methods can provide a valuable theoretical insight into the nature of quantum entanglement and nonlocality.

We report on experiments with transmon qubits using IBMQ²⁹ quantum processors to quantify Bell's nonlocality and the negativity of a two-qubit entangled state. We compared QST-based and multicopy (collective) methods. The potential of working with several copies of a system has been studied in a similar context of learning complex properties from experiments in Ref.³⁰. The collective approaches we utilize^{31,32} are based on a set of local Makhlin's unitary invariants^{33,34} to describe nonlocal properties. Each of the relevant invariants can be expressed as a combination of the expectation values of singlet-state projections conducted on a few copies of a given two-qubit system. The prepared copies of pairs of the entangled states must be exactly the same. This could be ensured by physically permuting the imperfect copies at random and averaging over the permutations. In linear optics, singlet projection is implemented through measuring the anticoalescence of two photons interfering on a balanced beam splitter, as in Hong-Ou-Mandel (HOM) setup³⁵. The singlet projection is implemented as a quantum circuit designed to distinguish between symmetric (coalescence) and antisymmetric (anticoalescence) Bell states.

We trained artificial neural networks (ANNs) to estimate entanglement and nonlocality from the top five experimental configurations for Werner's and Horodecki's states. As shown in Figure 4, the ANN output, based on a reduced set of projections, aligns with expected values and enhances noise robustness. The figure illustrates the model's performance and how the selected configurations contribute to the accuracy. This could simplify and improve the error-robustness of multicopy measurements without any complex nonlinear equation analysis.

Theoretical framework

The entanglement measure we investigate is the negativity, introduced by Życzkowski *et al.*³⁶, and later described in³⁷. For two qubits, it quantifies the cost of entanglement under operations that preserve the positivity of quantum circuits under partial transposition, known as PPT operations^{38,39}. This criterion is a quantitative version of the Peres-Horodecki separability criterion. For a two-qubit system, we can calculate negativity by finding the unique positive solution of the following equation⁴⁰:

$$a_4N^4 + a_3N^3 + a_2N^2 + a_1N + a_0 = 0, \quad (1)$$

where $a_0 = 48 \det \hat{\rho}^\Gamma$, $a_1 = 4(1 - 3\Pi_2 + 2\Pi_3)$, $a_2 = 6(1 - \Pi_2)$, $a_3 = 6$, and $a_4 = 3$. Here, $\Pi_n = \text{tr}[(\hat{\rho}^\Gamma)^n]$ are the moments of the partially transposed density matrix $\hat{\rho}^\Gamma$. The two-qubit negativity, as defined in³¹, is given by $N = 2\mu$, where μ represents the absolute value of the negative eigenvalue of $\hat{\rho}^\Gamma$. It was reported that solving Eq. (1) provides simpler formulas for the negativity than other equivalent approaches⁴¹.

The detection and quantification of the violation of Bell's nonlocality of two qubits is frequently carried out using the CHSH inequality. The measure of nonlocality corresponds to the degree of violation of this inequality, optimized for all measurement settings. The maximal degree of a CHSH inequality violation can be expressed as⁴²:

$$B = \text{tr} \hat{R} - \min[\text{eig}(\hat{R})] - 1, \quad (2)$$

where we use only the eigenvalues of the symmetric matrix $\hat{R} = \hat{\beta} \hat{\beta}^T$. Here, $\hat{\beta} = \text{tr}[(\hat{\sigma}_i \otimes \hat{\sigma}_j) \hat{\rho}]$ is a correlation matrix and $\hat{\sigma}_i$ for $i = 0, 1, 2, 3$ correspond to, respectively, the single-qubit identity matrix and the Pauli matrices. In the case of multiple copies, only six measurements are sufficient to determine the eigenvalues r_n for $n = 1, 2, 3$ of \hat{R} . Violation of the Bell-CHSH inequality occurs for positive values of B and, where the maximum $B = 1$ corresponds to maximally entangled states.

The spectrum of \hat{R} is given by the r roots of the following characteristic equation:

$$r^3 - \text{tr} \hat{R} r^2 - \frac{1}{2} [(\text{tr} \hat{R})^2 + \text{tr} \hat{R}^3] r - \frac{1}{6} \left\{ \text{tr} \hat{R}^3 + [6(\det \hat{\beta})^2 - (\text{tr} \hat{R})^3] \right\} = 0. \quad (3)$$

The polynomial parameters in Eqs. (1) and (3) can be related to the set of 18 local unitary invariants proposed in³³ to describe properties of a two-qubit system. We use these invariants to quantify entanglement and nonlocality in a manner that is independent of local unitary operations.

These invariants can be expressed as expectation values of measurements performed on a few copies of a two-qubit system³². In particular, by measuring the rate of the singlet-state projections, we can express each of the relevant invariants with averages over dichotomous measurements with values of ± 1 corresponding, respectively, to the odd/even number of singlet projections for a given measurement configuration. We represent the relevant invariants using three types of projection configurations, as defined in Ref.³². These include: (i) the local chained projections, where the singlet-state projections are performed independently for each subsystem: c_1, \dots, c_8 as demonstrated in Figs. 2(d); (ii) the local looped projections, which are similar to chained projections, but performed on all pairs of qubits: l_1, l_2 [see Figs. 2(b)]; and (iii) the cross-subsystem projections which are performed on qubits belonging to different subsystems: l_0 (the single-copy singlet-state projection), \bar{c}_1 , \bar{c}_2 , \bar{l}_1 , and \bar{l}_2 [see Figs. 2(e) and 2(c)].

The relevant invariants can be expressed in terms of rates of mutlicopy projections:

$$\begin{aligned} I_1 &= -\frac{8}{3} \left\{ l_0 [l_0(4l_0 - 3) + 6(\bar{c}_1 - 2\bar{l}_1)] + 3\bar{l}_1 - 6\bar{c}_2 + 8\bar{l}_2 \right\}, \\ I_2 &= 1 + 16l_1 - 4c_{12}, \\ I_3 &= 1 + 256l_2 - 128c_{45} + 64c_3 + 16(c_1^2 + c_2^2) - 8c_{12}, \end{aligned} \quad (4)$$

where $c_{ij} = c_i + c_j$. The coefficients a_0 , a_1 , and a_2 used in Eq. (1) are:

$$\begin{aligned} a_0 &= -16 [l_0^3 + 2\bar{l}_2 + 3(l_1^2 - l_0^2 \bar{c}_1 - l_0 \bar{l}_1 + \bar{c}_1 \bar{l}_1) - 6(l_2 - l_0 \bar{c}_2 + \bar{c}_3)], \\ a_1 &= 24 [l_0^2 - \bar{l}_1 - l_1 + 2(c_3 - l_0 \bar{c}_1 + \bar{c}_2)] - 32 (l_0^3 - 3l_0 \bar{l}_1 + 2\bar{l}_2), \\ a_2 &= 12 (c_{12} - 2l_1). \end{aligned} \quad (5)$$

We can reformulate Eq. (2) to assess the Bell's nonlocality measure as:

$$B = I_2 - \min(r) - 1, \quad (6)$$

where r are the roots of:

$$r^3 - I_2 r^2 + \frac{1}{2} (I_2^2 - I_3) r + \frac{1}{6} [I_2^3 + (6I_1^2 - I_2^3)]. \quad (7)$$

Experiment

In our experiments, we use two approaches towards quantifying nonlocality and entanglement, i.e., QST and the invariants-based approach. We test these methods on two single-parameter classes of states, i.e., Werner's states, $\hat{\rho}^{\mathcal{W}}(p) = p|\Psi^-\rangle\langle\Psi^-| + (1-p)\mathbb{1}/4$, and Horodecki's states, $\hat{\rho}^{\mathcal{H}}(p) = p|\Psi^-\rangle\langle\Psi^-| + (1-p)|00\rangle\langle 00|$, which are given in terms of the singlet state $|\Psi^-\rangle = \frac{1}{\sqrt{2}}(|01\rangle - |10\rangle)$, $p \in [0, 1]$, and $\mathbb{1}/4$ describes white noise. These states are designed to have extreme amount of entanglement for a given degree of CHSH violation and are known to be challenging to prepare and characterize in the presence of noise. To perform the submeasurements required to determine Makhlin's invariants, we created the quantum circuits composed of the block shown in Fig. 6. For details, see the Supplemental Information⁴³. The results for the Werner's and Horodecki's states (see Fig. 3) were obtained by first running simulations with the *ibmq_qasm_simulator* simulator and then running physical quantum circuits on the *ibm_hanoi* quantum processor²⁹. The calibration details for the quantum processor are given in⁴³.

Due to the statistical fluctuations in the measured data, we occasionally observe a configuration of parameters that is not explained by a physical model. To find most of the parameter values that are both physical and make the observed data most probable, we apply Maximum Likelihood Estimation (MLE). This approach is widely used and accepted in QST⁴⁴ to deal with similar problems, i.e., the elements of a density matrix measured directly^{45,46} may result in a matrix that is not positive semidefinite. MLE is then used to find the most likely positive semidefinite matrix associated with the observed parameters. This normalized positive semidefinite matrix represents the physical model which is fitted using the MLE. The likelihood function is then a quadratic function of the density matrix parameters. This simplifies the MLE problem making it easier to solve numerically. We measure multicopy observables, with the likelihood function being a polynomial of the single-copy density matrix elements. This function is proportional to the sum of logarithms of detection rates for different experimental configurations. These probabilities are obtained from a normal distribution, where the mean corresponds to the event rate observed in the experiment and the variance is estimated as the square root of the rate. Here, the optimization is more challenging than for QST as the likelihood function is no longer quadratic, i.e., many density matrices can result in the same set of the observed values and the same value of the likelihood function. We expect the measured quantities to be invariant with respect to local unitary operations. Thus, we reduce the number of the parameters of the density matrix model to exclude phase factors, i.e., we only work with real-valued density matrices. This is justified because in our case all phase factors can be set to zero by local unitary operations. This reduces the size of the parameter space and makes the MLE method to converge to the desired solution much faster. However, we are left with an unknown set of local operations that would provide complete information about the density matrix. Due to the polynomial nature of the likelihood function, there could be some ambiguity regarding the solution to the MLE problem, however, we did not find this to be an issue in our experiments. Our MLE calculations give consistent results for various initial configurations of the optimization problem.

To analyze the contributions of individual projections to the final outcome of the entanglement witnesses and measures, we used a game theoretic approach (i.e., SHAP⁴⁷) explaining the output of any AI model. The SHAP concept involves: establishing a baseline prediction, permuting feature values, and calculating Shapley values by comparing model predictions with and without each feature. This process sheds light on the contribution of each feature. Detailed SHAP analyses are provided in the Supplemental Information⁴³ (see Figs. 7). In an examination of 5×10^5 randomly selected input states, our results are consistent with the analytical expressions for the negativity [see Eqs. (1) and (5)], which are independent of c_4 and c_5 . Similarly, for nonlocality we can ignore \bar{c}_3 [see Eq. (7) and (4)]. Focusing on specific classes of states, such as Werner's states, it becomes evident that a substantially reduced number of projections, namely five, suffices.

On the other hand, for Horodecki's states, the SHAP analysis reveals a notable impact of a higher number of projections. This aligns with established challenges in experimental settings associated with the complexity of preparing and characterizing Horodecki's states.

In case of the Werner states the projections corresponding to l_1 , \bar{l}_1 , l_2 , and \bar{l}_2 are symmetric, as can also be seen in the analysis of the impact of these measurements on the value of the entanglement or nonlocality measures. Leveraging these crucial insights into state-specific projections, we trained the ANNs to estimate the entanglement and nonlocality measures based on the five most significant submeasurements. This was carried out for the Werner and Horodecki states, respectively. The output of the trained ANN on the reduced set of projections corresponds to the expected entanglement and nonlocality values and improves the noise robustness of our method. This suggests that the same approach can be used to reduce the complexity and improve the error-robustness of the entanglement or nonlocality measurement for other classes of states without having to analyze complex sets of nonlinear equations.

Conclusions

Our experimental results demonstrate the effectiveness of the proposed approach for quantifying entanglement properties in two-qubit mixed states without resorting to resource-intensive quantum state tomography. By employing the method of singlet

projections through HOM interference, we successfully determined local Makhlin's invariants, which indicate nonclassical features, such as Bell's nonlocality and entanglement. Our experiments utilized quantum processors to implement shallow quantum circuits (shown in Figs. 6 and 5 in⁴³) inspired by the Hong–Ou–Mandel interference approach to entanglement quantification. Our comparison with the traditional QST approach demonstrates the efficiency of our method, which required a significantly fewer measurements while providing accurate estimations of the entanglement properties. Notably, we applied our approach to various two-qubit Werner's states and Horodecki's states, and obtained consistent and reliable results. These results contribute to the advancement of experimental techniques for quantifying and characterizing quantum entanglement and nonlocality in practical quantum systems, offering a more streamlined alternative to conventional methods. In particular, we have demonstrated that applying a maximum likelihood method to the multicopy measurements mitigates the experimental noise to an acceptable level, allowing quantum entanglement to be determined independently of the local unitary operations applied to the entangled subsystems under investigation. The noise can be suppressed even further if we consider performing only state-specific measurements, as demonstrated by our SHAP–ANN–based approach.

We have demonstrated that implementing neural networks trained on a reduced set of singlet projections improves the robustness of entanglement and nonlocality measurements. This suggests that by reducing the number of the experimental configurations, the measurement process can be simplified, enhancing fault tolerance and making the approach more practical for complex quantum systems. Our analysis shows that using only a subset of projection configurations is sufficient, allowing for significant experimental optimization.

We hope that these results could stimulate further research into the measurement of nonlinear quantum properties, in particular entanglement and nonlocality, without the need for full QST. Our results highlight the potential to streamline the measurement process by circumventing exhaustive QST, and show that it is possible to implement that method on real devices. These results offer a promising direction for the development of more efficient and effective AI-assisted experimental techniques in the field of quantum systems' analysis.

In summary, our work represents a significant advance in the measurement of quantum entanglement and nonlocality. By demonstrating an AI-assisted multicopy approach, we offer an alternative to traditional methods that requires fewer measurement resources. This approach not only simplifies the measurement process but also leads to more accurate and efficient characterization of quantum systems. Our research shows that using maximum likelihood estimation (MLE) within the multicopy approach increases noise tolerance, addressing a critical challenge in practical quantum measurements. By providing a more practical way to measure complex quantum properties, our results could lead to the development of advanced quantum protocols that exploit entanglement and nonlocal correlations, with potential applications in practical quantum communication and computing.

Data and code availability

All relevant data and code supporting the document is available upon request. Please refer to Patrycja Tulewicz at patul@amu.edu.pl.

References

1. Schrödinger, E. Discussion of Probability Relations between Separated Systems. *Math. Proc. Camb. Phil. Soc.* **31**, 555, [10.1017/S0305004100013554](https://doi.org/10.1017/S0305004100013554) (1935).
2. Einstein, A., Podolsky, B. & Rosen, N. Can quantum-mechanical description of physical reality be considered complete? *Phys. Rev.* **47**, 777–780, [10.1103/PhysRev.47.777](https://doi.org/10.1103/PhysRev.47.777) (1935).
3. Horodecki, R., Horodecki, P., Horodecki, M. & Horodecki, K. Quantum entanglement. *Rev. Mod. Phys.* **81**, 865–942, [10.1103/RevModPhys.81.865](https://doi.org/10.1103/RevModPhys.81.865) (2009).
4. Bell, J. S. On the Einstein–Podolsky–Rosen paradox. *Phys. (Long Island City, New York)* **1** (1964).
5. Bell, J. S. & Aspect, A. *Speakable and Unsayable in Quantum Mechanics: Collected Papers on Quantum Philosophy* (Cambridge University Press, 2004), 2 edn.
6. Brunner, N., Cavalcanti, D., Pironio, S., Scarani, V. & Wehner, S. Bell nonlocality. *Rev. Mod. Phys.* **86**, 419–478, [10.1103/RevModPhys.86.419](https://doi.org/10.1103/RevModPhys.86.419) (2014).
7. Nielsen, M. A. & Chuang, I. L. *Quantum Computation and Quantum Information* (Cambridge University Press, 2010).
8. de Riedmatten, H. *et al.* Long distance quantum teleportation in a quantum relay configuration. *Phys. Rev. Lett.* **92**, 047904, [10.1103/PhysRevLett.92.047904](https://doi.org/10.1103/PhysRevLett.92.047904) (2004).
9. Ekert, A. K. Quantum cryptography based on Bell's theorem. *Phys. Rev. Lett.* **67**, 661–663, [10.1103/PhysRevLett.67.661](https://doi.org/10.1103/PhysRevLett.67.661) (1991).

10. Cleve, R. & Buhrman, H. Substituting quantum entanglement for communication. *Phys. Rev. A* **56**, 1201–1204, [10.1103/PhysRevA.56.1201](https://doi.org/10.1103/PhysRevA.56.1201) (1997).
11. Mayers, D. & Yao, A. C.-C. Quantum cryptography with imperfect apparatus. *Proc. 39th Annu. Symp. on Foundations Comput. Sci. (Cat. No.98CB36280)* 503–509 (1998).
12. Acín, A. *et al.* Device-independent security of quantum cryptography against collective attacks. *Phys. Rev. Lett.* **98**, 230501, [10.1103/PhysRevLett.98.230501](https://doi.org/10.1103/PhysRevLett.98.230501) (2007).
13. Park, H. S., Lee, S.-S. B., Kim, H., Choi, S.-K. & Sim, H.-S. Construction of an optimal witness for unknown two-qubit entanglement. *Phys. Rev. Lett.* **105**, 230404, [10.1103/PhysRevLett.105.230404](https://doi.org/10.1103/PhysRevLett.105.230404) (2010).
14. Horodecki, P. & Ekert, A. Method for direct detection of quantum entanglement. *Phys. Rev. Lett.* **89**, 127902, [10.1103/PhysRevLett.89.127902](https://doi.org/10.1103/PhysRevLett.89.127902) (2002).
15. Horodecki, P. Measuring quantum entanglement without prior state reconstruction. *Phys. Rev. Lett.* **90**, 167901, [10.1103/PhysRevLett.90.167901](https://doi.org/10.1103/PhysRevLett.90.167901) (2003).
16. Bovino, F. A. *et al.* Direct measurement of nonlinear properties of bipartite quantum states. *Phys. Rev. Lett.* **95**, 240407, [10.1103/PhysRevLett.95.240407](https://doi.org/10.1103/PhysRevLett.95.240407) (2005).
17. Rudnicki, L., Horodecki, P. & Życzkowski, K. Collective uncertainty entanglement test. *Phys. Rev. Lett.* **107**, 150502, [10.1103/PhysRevLett.107.150502](https://doi.org/10.1103/PhysRevLett.107.150502) (2011).
18. Lemr, K., Bartkiewicz, K. & Černoch, A. Experimental measurement of collective nonlinear entanglement witness for two qubits. *Phys. Rev. A* **94**, 052334, [10.1103/PhysRevA.94.052334](https://doi.org/10.1103/PhysRevA.94.052334) (2016).
19. Koutný, D. *et al.* Deep learning of quantum entanglement from incomplete measurements. *Sci. Adv.* **9**, eadd7131, [10.1126/sciadv.add7131](https://doi.org/10.1126/sciadv.add7131) (2023).
20. Feng, C. & Chen, L. Quantifying quantum entanglement via machine learning models. *Commun. Theor. Phys.* (2024).
21. Pan, G.-Z. *et al.* Quantifying entanglement for unknown quantum states via artificial neural networks. *Sci. Reports* **14**, 26267, [10.1038/s41598-024-76978-7](https://doi.org/10.1038/s41598-024-76978-7) (2024).
22. Clauser, J. F., Horne, M. A., Shimony, A. & Holt, R. A. Proposed experiment to test local hidden-variable theories. *Phys. Rev. Lett.* **23**, 880–884, [10.1103/PhysRevLett.23.880](https://doi.org/10.1103/PhysRevLett.23.880) (1969).
23. Freedman, S. J. & Clauser, J. F. Experimental test of local hidden-variable theories. *Phys. Rev. Lett.* **28**, 938–941, [10.1103/PhysRevLett.28.938](https://doi.org/10.1103/PhysRevLett.28.938) (1972).
24. Aspect, A., Grangier, P. & Roger, G. Experimental tests of realistic local theories via Bell’s theorem. *Phys. Rev. Lett.* **47**, 460–463, [10.1103/PhysRevLett.47.460](https://doi.org/10.1103/PhysRevLett.47.460) (1981).
25. Aspect, A., Grangier, P. & Roger, G. Experimental realization of Einstein-Podolsky-Rosen-Bohm gedankenexperiment: A new violation of Bell’s inequalities. *Phys. Rev. Lett.* **49**, 91–94, [10.1103/PhysRevLett.49.91](https://doi.org/10.1103/PhysRevLett.49.91) (1982).
26. Aspect, A., Dalibard, J. & Roger, G. Experimental test of Bell’s inequalities using time-varying analyzers. *Phys. Rev. Lett.* **49**, 1804–1807, [10.1103/PhysRevLett.49.1804](https://doi.org/10.1103/PhysRevLett.49.1804) (1982).
27. Peres, A. Separability criterion for density matrices. *Phys. Rev. Lett.* **77**, 1413–1415, [10.1103/PhysRevLett.77.1413](https://doi.org/10.1103/PhysRevLett.77.1413) (1996).
28. Horodecki, M., Horodecki, P. & Horodecki, R. Separability of mixed states: necessary and sufficient conditions. *Phys. Lett. A* **223**, 1–8, [https://doi.org/10.1016/S0375-9601\(96\)00706-2](https://doi.org/10.1016/S0375-9601(96)00706-2) (1996).
29. IBM Quantum. <https://www.ibm.com/quantum> (2024).
30. Huang, H.-Y. *et al.* Quantum advantage in learning from experiments. *Science* **376**, 1182–1186, [10.1126/science.abn7293](https://doi.org/10.1126/science.abn7293) (2022).
31. Bartkiewicz, K., Chimczak, G. & Lemr, K. Direct method for measuring and witnessing quantum entanglement of arbitrary two-qubit states through Hong-Ou-Mandel interference. *Phys. Rev. A* **95**, 022331, [10.1103/PhysRevA.95.022331](https://doi.org/10.1103/PhysRevA.95.022331) (2017).
32. Bartkiewicz, K. & Chimczak, G. Two methods for measuring Bell nonlocality via local unitary invariants of two-qubit systems in Hong-Ou-Mandel interferometers. *Phys. Rev. A* **97**, 012107, [10.1103/PhysRevA.97.012107](https://doi.org/10.1103/PhysRevA.97.012107) (2018).
33. Makhlin, Y. Nonlocal properties of Two-Qubit gates and mixed states, and the optimization of quantum computations. *Quantum Inf. Process.* **1**, 243–252, [10.1023/a:1022144002391](https://doi.org/10.1023/a:1022144002391) (2002).
34. Grassl, M., Rötteler, M. & Beth, T. Computing local invariants of quantum-bit systems. *Phys. Rev. A* **58**, 1833–1839, [10.1103/PhysRevA.58.1833](https://doi.org/10.1103/PhysRevA.58.1833) (1998).

35. Hong, C. K., Ou, Z. Y. & Mandel, L. Measurement of subpicosecond time intervals between two photons by interference. *Phys. Rev. Lett.* **59**, 2044–2046, [10.1103/PhysRevLett.59.2044](https://doi.org/10.1103/PhysRevLett.59.2044) (1987).
36. Życzkowski, K., Horodecki, P., Sanpera, A. & Lewenstein, M. Volume of the set of separable states. *Phys. Rev. A* **58**, 883–892, [10.1103/PhysRevA.58.883](https://doi.org/10.1103/PhysRevA.58.883) (1998).
37. Vidal, G. & Werner, R. F. Computable measure of entanglement. *Phys. Rev. A* **65**, 032314, [10.1103/PhysRevA.65.032314](https://doi.org/10.1103/PhysRevA.65.032314) (2002).
38. Audenaert, K., Plenio, M. B. & Eisert, J. Entanglement cost under positive-partial-transpose-preserving operations. *Phys. Rev. Lett.* **90**, 027901, [10.1103/PhysRevLett.90.027901](https://doi.org/10.1103/PhysRevLett.90.027901) (2003).
39. Ishizaka, S. Binegativity and geometry of entangled states in two qubits. *Phys. Rev. A* **69**, 020301, [10.1103/PhysRevA.69.020301](https://doi.org/10.1103/PhysRevA.69.020301) (2004).
40. Bartkiewicz, K., Beran, J., Lemr, K., Norek, M. & Miranowicz, A. Quantifying entanglement of a two-qubit system via measurable and invariant moments of its partially transposed density matrix. *Phys. Rev. A* **91**, 022323, [10.1103/PhysRevA.91.022323](https://doi.org/10.1103/PhysRevA.91.022323) (2015).
41. Miranowicz, A. *et al.* Statistical mixtures of states can be more quantum than their superpositions: Comparison of nonclassicality measures for single-qubit states. *Phys. Rev. A* **91**, 042309, [10.1103/PhysRevA.91.042309](https://doi.org/10.1103/PhysRevA.91.042309) (2015).
42. Horodecki, M., Horodecki, P. & Horodecki, R. Separability of mixed states: necessary and sufficient conditions. *Phys. Lett. A* **223**, 1–8, [10.1016/s0375-9601\(96\)00706-2](https://doi.org/10.1016/s0375-9601(96)00706-2) (1996).
43. See Supplemental Information at URL-will-be-inserted-by-publisher for the data of the experiments.
44. James, D. F. V., Kwiat, P. G., Munro, W. J. & White, A. G. Measurement of qubits. *Phys. Rev. A* **64**, 052312, [10.1103/PhysRevA.64.052312](https://doi.org/10.1103/PhysRevA.64.052312) (2001).
45. Bartkiewicz, K., Černoč, A., Lemr, K. & Miranowicz, A. Priority choice experimental two-qubit tomography: Measuring one by one all elements of density matrices. *Sci. Rep.* **6**, 19610, [10.1038/srep19610](https://doi.org/10.1038/srep19610) (2016).
46. Miranowicz, A. *et al.* Optimal two-qubit tomography based on local and global measurements: Maximal robustness against errors as described by condition numbers. *Phys. Rev. A* **90**, 062123, [10.1103/PhysRevA.90.062123](https://doi.org/10.1103/PhysRevA.90.062123) (2014).
47. Lundberg, S. M. & Lee, S.-I. A unified approach to interpreting model predictions. In Guyon, I. *et al.* (eds.) *Advances in Neural Information Processing Systems 30*, 4765–4774 (Curran Associates, Inc., 2017).
48. Cross, A. W., Bishop, L. S., Sheldon, S., Nation, P. D. & Gambetta, J. M. Validating quantum computers using randomized model circuits. *Phys. Rev. A* **100**, 032328, [10.1103/PhysRevA.100.032328](https://doi.org/10.1103/PhysRevA.100.032328) (2019).
49. Qiskit contributors. Qiskit: An open-source framework for quantum computing, [10.5281/zenodo.2573505](https://doi.org/10.5281/zenodo.2573505) (2023).

Acknowledgements

P.T, K.B, A.M are supported by the Polish National Science Center from funds awarded through the Maestro Grant No. DEC-2019/34/A/ST2/00081. F.N. is supported in part by: Nippon Telegraph and Telephone Corporation (NTT) Research, the Japan Science and Technology Agency (JST) [via the CREST Quantum Frontiers program Grant No. JPMJCR24I2, the Quantum Leap Flagship Program (Q-LEAP), and the Moonshot R&D Grant Number JPMJMS2061], and the Office of Naval Research (ONR) Global (via Grant No. N62909-23-1-2074).

Author contributions statement

K.B. conceived the project, supervised the work and developed MLE for multicopy experiments. P.T. designed and performed the experiments, numerical calculations, and developed the ANN model. P.T. and K.B. performed analysis of the results and wrote the manuscript. All authors contributed to the discussions and interpretations of the results and reviewed the manuscript.

Competing interests

The authors declare no competing interests.

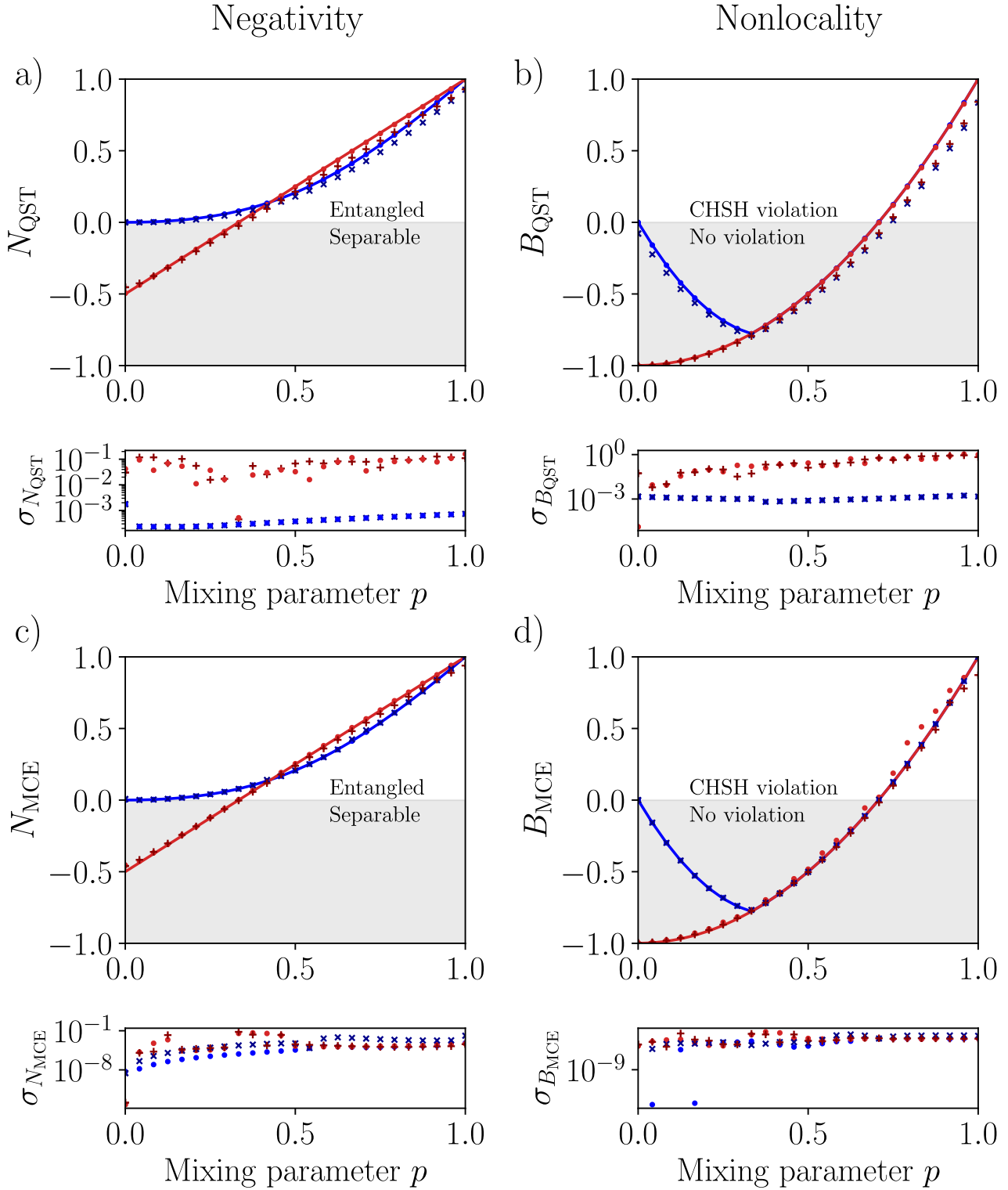


Figure 3. Experimental quantification of entanglement (left column) and nonlocality (right column) for Werner and Horodecki states, determined by measuring the negativity N and Bell nonlocality B as a function of the mixing parameter p . Solid curves show theoretical predictions for ideal states. The results were obtained using: (a, b) quantum state tomography (QST), and (c, d) multicopy estimation (MCE). Assumptions include shot noise (● for Werner states, ● for Horodecki states) using *ibmq_qasm_simulator*, and experimental data (+ for Werner states, × for Horodecki states) collected with the quantum processor *ibm_hanoi*. Standard deviations σ were estimated by simulating 10^5 experiments for ideal and noisy circuits, with noise models based on calibration data.

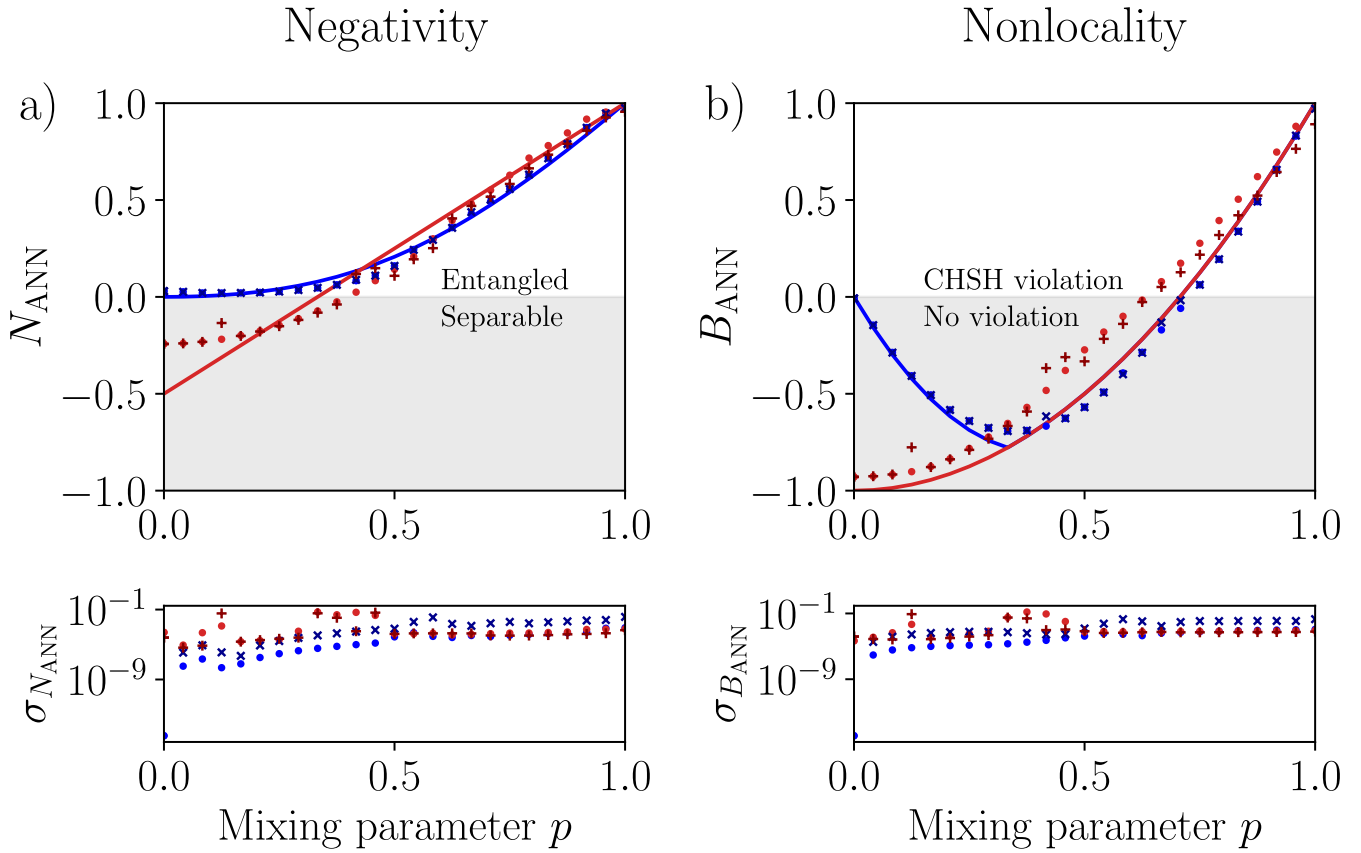


Figure 4. Same as in Fig.3, but for the ANN trained on the random input states and a limited set of the singlet projections, including only the five top significant projections, as revealed by the SHAP analysis (see Fig. 7 in⁴³). Assumptions include shot noise (● for Werner states, ● for Horodecki states) using *ibmq_qasm_simulator*, and experimental data (+ for Werner states, × for Horodecki states) collected with the quantum processor *ibm_hanoi*.

Supplementary

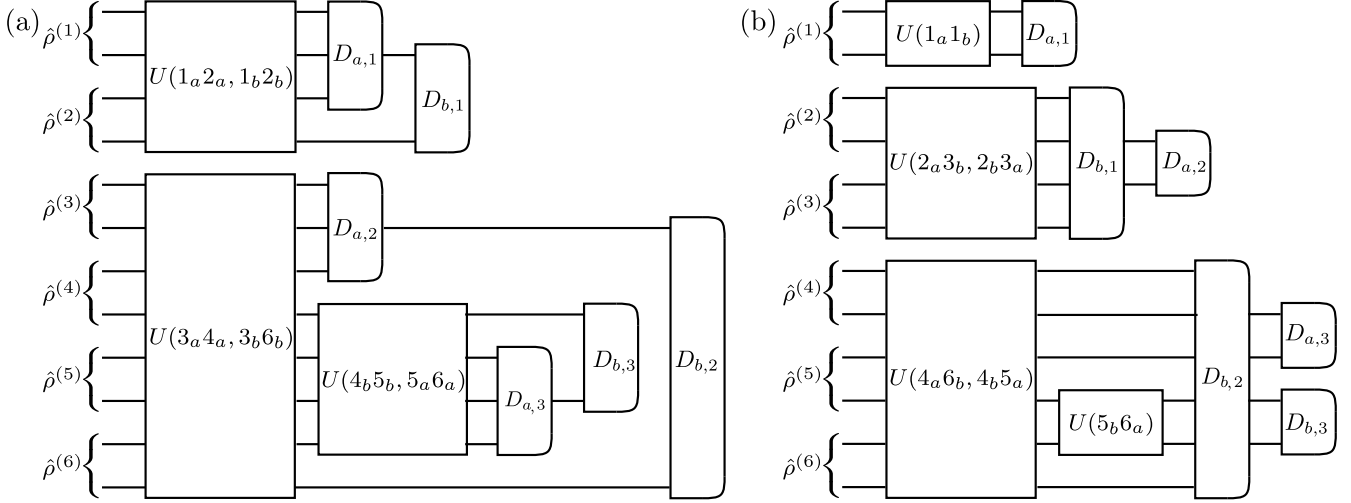


Figure 5. Circuits configurations for measuring all independent singlet projections. In the configuration (a) the circuit can measure $l_1, l_2, c_1, c_2, c_3, \bar{c}_3, c_4$, and c_5 ; and in the configuration (b) $l_0, \bar{c}_1, \bar{c}_2, \bar{l}_1$, and \bar{l}_2 . The $U(k_a k_b)$ and $U(k_a l_b | l_a k_b)$ gates are shown in Figs. 6 (a) and (b) respectively. Pairs of the detectors $D_{a,n}$ and $D_{b,n}$, for $n = 1, 2, 3$, measure coalescence or anticoalescence. The sum of coalescence and anticoalescence is given as $s = a + c$ and is proportional to the incidence rate of photon pairs. Depending on the measured quantity, we choose the appropriate circuit and counts. The relation between the counts and the particular singlet projections for circuits (a) and (b) is shown in Table 1.

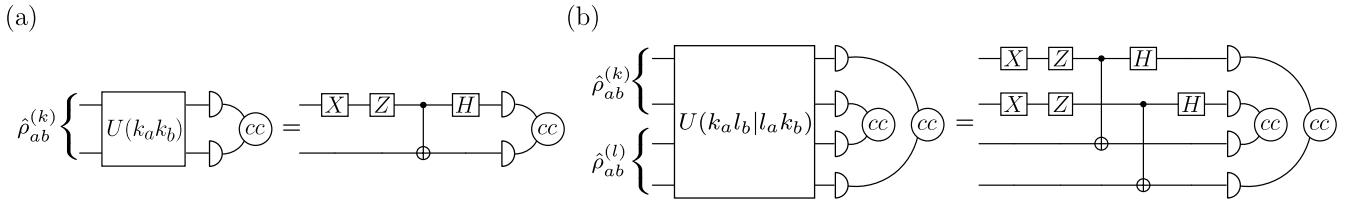


Figure 6. Circuits realizing the singlet projections: (a) $U(k_a k_b)$ on the k th pair of entangled qubits in the state $\hat{\rho}_{a,b}^{(k)}$, and (b) $U(k_a l_b | l_a k_b)$ on two copies of pairs of qubits from the subsystems a and b , i.e., $\hat{\rho}_{a,b}^{(k)}$ and $\hat{\rho}_{a,b}^{(l)}$.

Our experiments were implemented on the *ibm_hanoi*²⁹ processor, which a twenty–seven qubit IBM Quantum Falcon Processor (Falcon r5.11L)²⁹ operating with Quantum Volume (as defined in Ref.⁴⁸) of 64. The crucial parameters of the processor qubits were calibrated during the course of the experiment are shown in Fig. 9. We used the *Sampler* primitive given by *Qiskit Runtime* program, which provides a matrix–free measurement mitigation (M3)⁴⁹ routine to mitigate errors, of our experiment. To confirm that the maximum number of shots per circuit (10^6) was sufficient, we compared this value with the results depicted in Fig. 8. We also tested if this configuration provides a reasonable accuracy for a random two-qubit input state, as shown in Table 2.

Table 1. Table relating the measurement configurations to their interpretations for the circuits shown in Fig. 5.

Detectors						Circuits	
$D_{a,1}$	$D_{a,2}$	$D_{a,3}$	$D_{b,1}$	$D_{b,2}$	$D_{b,3}$	(a)	(b)
a	s	s	a	s	s	l_1	—
s	a	a	s	a	a	l_2	—
s	s	s	s	s	a	c_1	—
s	s	a	s	s	s	c_2	—
s	a	s	s	a	s	c_3	—
s	s	a	s	a	a	\bar{c}_3	—
s	s	s	a	a	a	c_4	—
s	a	s	s	a	a	c_5	—
a	s	s	s	s	s	—	l_0
s	s	s	a	s	s	—	\bar{c}_1
s	s	s	s	a	a	—	\bar{c}_2
s	a	s	a	s	s	—	\bar{l}_1
s	s	a	s	a	a	—	\bar{l}_2

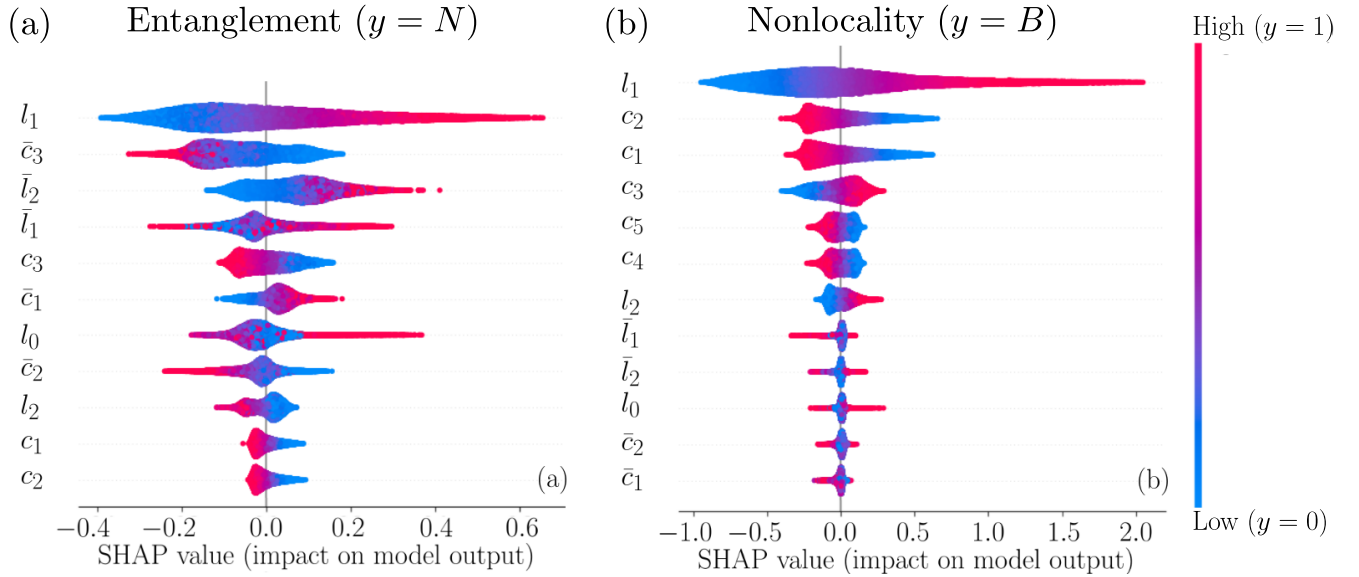


Figure 7. SHAP analysis for 5×10^5 random input states for (a) the negativity N and (b) nonlocality B measures predicted by the exact formulas. The impact of the required detection rates of the specific singlet projections affects the feature value $y = B, N$ of the particular ANN in different ways. Here, these relations are represented graphically and are used to select the most significant projections for the 5-parameter ANN models discussed in the main text.

Table 2. Table showing measurements for a random input state $|\Psi\rangle$. Measurements were simulated on the *QasmSimulator* simulator assuming the typical noise of the quantum processor used in our experiments, and *ibm_brisbane* quantum processor. The state is given by $|\Psi\rangle = [-0.0104 + 0.2758i, -0.6451 + 0.1559, 0.03716 - 0.0168i, 0.11874 + 0.6838i]^T$.

Variable	Theory	Simulator				<i>ibm_brisbane</i>			
		QST (with MLE)	MCE (no MLE)	MCE (with MLE)	ANN	QST (with MLE)	MCE (no MLE)	MCE (with MLE)	ANN
I_1	-0.1138	-0.1131	-0.113	-0.1064	-	-0.1101	0.6263	-0.1019	-
I_2	1.2277	1.2253	1.2306	1.2119	-	1.1495	1.0856	1.1022	-
I_3	1.026	1.0235	0.8093	1.0208	-	0.8716	0.6985	0.8053	-
N	0.3374	0.3361	0.3466	0.326	0.3139	0.3186	0.198	0.3018	0.3022
B	0.1138	0.1123	0.1884	0.1056	0.114	0.0428	0.1267	0.0062	0.0027

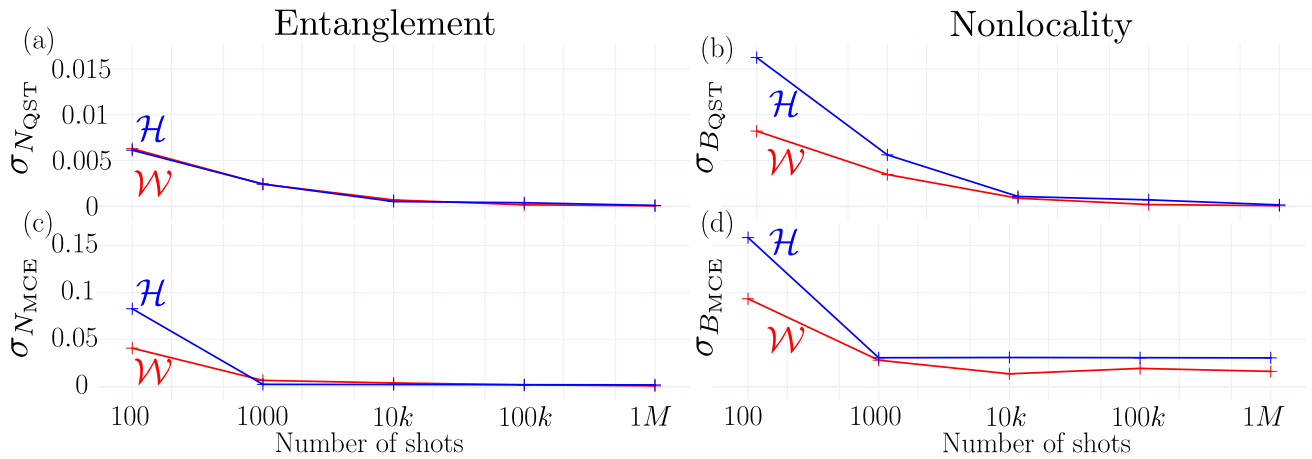


Figure 8. Standard deviations of the negativity N (left column) and nonlocality B (right) measurements computed for perfect circuits, for the (a,b) QST and (c,d) MCE methods, for the Werner (\mathcal{W}) and Horodecki (\mathcal{H}) states as functions of the number of shots.

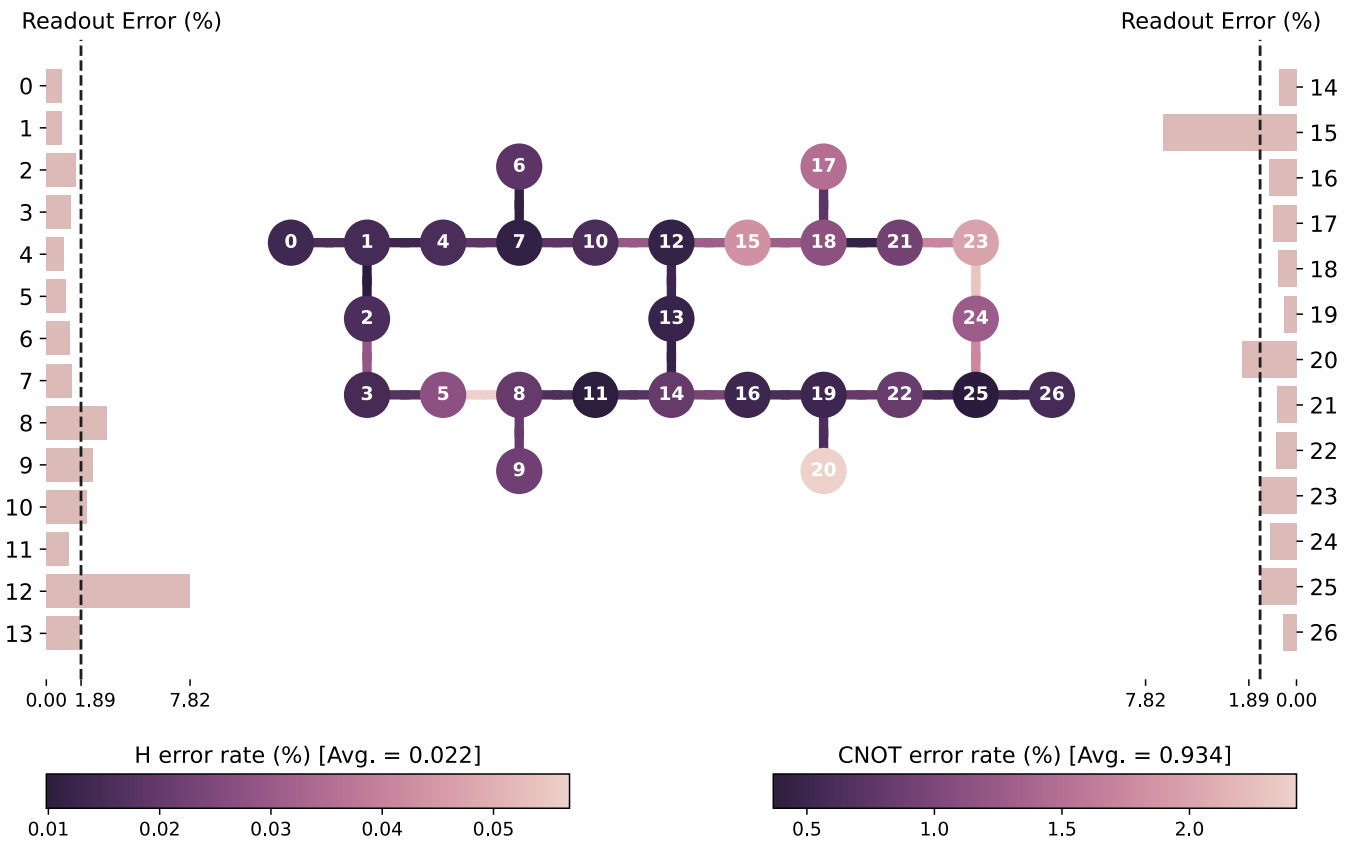


Figure 9. Error rate parameters of the *ibm_hanoi* 27-qubits processor²⁹ calibrated for our experiment. Depending on the number of qubits needed for particular projections, the transpiler set the selection of qubits from the set $\{1 - 5, 7, 10, 12 - 14, 16, 19\}$.